Metastable States and Wetting Transition of Submerged Superhydrophobic Structures

Pengyu Lv,[1] Yahui Xue,[1] Yipeng Shi,[1,2] Hao Lin,[3,*] and Huiling Duan[1,2,†]
[1]State Key Laboratory for Turbulence and Complex Systems, Department of Mechanics and Engineering Science, College of Engineering, Peking University, Beijing 100871, China
[2]Key Laboratory of High Energy Density Physics Simulation, Center for Applied Physics and Technology, Peking University, Beijing 100871, China
[3]Mechanical and Aerospace Engineering, Rutgers, The State University of New Jersey, 98 Brett Road, Piscataway, New Jersey 08854, USA

(Received 30 December 2013; revised manuscript received 10 March 2014; published 12 May 2014)

Superhydrophobicity on structured surfaces is frequently achieved via the maintenance of liquid-air interfaces adjacent to the trapped air pockets. These interfaces, however, are subject to instabilities due to the Cassie-Baxter-to-Wenzel transition and total wetting. The current work examines *in situ* liquid-air interfaces on a submerged surface patterned with cylindrical micropores using confocal microscopy. Both the pinned Cassie-Baxter and depinned metastable states are directly observed and measured. The metastable state dynamically evolves, leading to a transition to the Wenzel state. This process is extensively quantified under different ambient pressure conditions, and the data are in good agreement with a diffusion-based model prediction. A similarity law along with a characteristic time scale is derived which governs the lifetime of the air pockets and which can be used to predict the longevity of underwater superhydrophobicity.

DOI: 10.1103/PhysRevLett.112.196101 PACS numbers: 68.08.Bc, 47.61.-k, 68.35.Ct

Structured superhydrophobic surfaces have attracted a lot of attention because of their broad applications in both engineering and sciences [1–4]. One key mechanism to realize their functionality is to maintain on such surfaces a large area fraction of liquid-gas interfaces in the pinned Cassie-Baxter (CB) state [5]. These interfaces, however, are subject to instabilities induced by mechanisms including vibration [6], evaporation [7,8], air diffusion [9–11], and impact [12,13], which are known to collapse the meniscus, leading to the fully wetted Wenzel (W) state and loss of superhydrophobicity [14]. Furthermore, the transition from the CB to W state is not always instantaneous and may occur gradually on a variable time scale [8–11,15–18]. The presence of the transient metastable states has been postulated by theoretical predictions and confirmed by experimental observations [10,17,19–23]. Understanding the CB-W transition and the dynamic evolution of the metastable state is critical for the regulation and improvement of CB-based superhydrophobicity. For example, structural design can be pursued to maximize the life span of the metastable state such as to extend the longevity of the superhydrophobic functionality [24]. On the other hand, residual gas in the metastable or nano-Cassie states also provides the possibility to recover the CB state by gas or vapor generation [25–27], local pressure regulation [28–30], or vibrations [31].

Various optical techniques have been used to observe the CB-W transition and metastable states in two typical situations, namely, droplet impalement onto surface microstructures [15–18] and air film (or plastron) decay at submerged superhydrophobic surfaces [9–11,28–30]. The former is believed to be induced by evaporation [15–17], and the evolution of the sinking meniscus has been quantified in three dimensions [17]. The latter is, in general, correlated with air diffusion [9,10]. Although previous attempts have been made to capture the dynamic transition process [9–11,28,30] (e.g., on disordered microstructured surfaces [10]), a controlled, sufficiently resolved measurement to establish quantitative understanding is currently absent and is the scope of the current work.

We use laser scanning confocal microscopy to investigate and quantify the CB-W transition and metastable states on regularly patterned surfaces submerged in water. Compared with indirect observation methods, such as light reflection [9,11,15,28] and transmission diffraction [30], the current technique can be used to dynamically resolve the liquid-air interfaces [10,17,18,29,32] and is, therefore, an ideal tool for the observation of the metastable state. We present the first controlled and detailed quantification of metastable states via *in situ* observation of submerged structures. In particular, we record the dynamic progress of the liquid-gas interface under different pressure conditions. The extensive data provide the necessary details for us to establish a diffusion-based model [22,33–36]. Importantly, we discover a similarity behavior which collapses the experimental data, as well as a simple time scale governing the life span of the metastable states. The results can, thus, serve as a convenient tool for the prediction and design of structure-enabled underwater superhydrophobicity.

The experimental setup is shown in Fig. 1. Samples patterned with cylindrical micropores [Figs. 1(b) and 1(c)] were obtained by photolithography and deep reactive ion

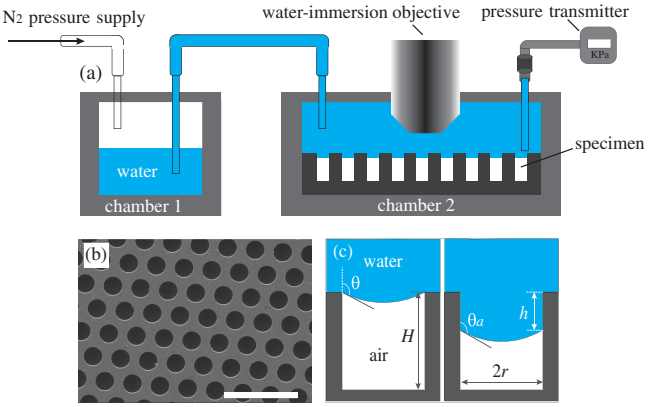

FIG. 1 (color online). (a) Schematics of the experiment setup. Hydrostatic pressure is supplied by compressing nitrogen up to 1.5 atm and is monitored by a pressure transmitter at the sample surface. The tube connecting chambers 1 and 2 is 1 m in length and 4 mm in diameter. The meniscus profile is measured by confocal microscopy. (b) Scanning electron microscopic images showing the pore-patterned surface. Each pore has a radius of $r = 25$ μm and a depth of $H = 40$ μm. The scale bar is 200 μm. (c) Schematics of the pinned Cassie-Baxter and depinned metastable states.

etching on silicon substrates, which were further coated with self-assembled monolayers of fluorosilanes to achieve hydrophobicity. A specimen was mounted on the bottom of a sealed plexiglass box and gradually submerged in deionized water, which, prior to each experiment, had been equilibrated in a clean ambient environment for approximately two days. Hydrostatic pressure (denoted by p_L) was applied by controlling the inlet nitrogen pressure which ranges from 1 to 50 kPa above the atmospheric pressure (denoted by p_0). The pressure difference is denoted by $\Delta p = p_L - p_0$. All the experiments were carried out at a constant temperature of 22 ± 1 °C.

Optical observation was made with a Carl Zeiss laser scanning confocal microscope (LSM 710, Carl Zeiss, Germany) using a 20× water immersion objective (NA= 1.0) with a 1.8 mm working distance. Two imaging modes were employed. In the first, a 3D configuration of the meniscus under liquid pressure can be reconstructed by a series of Z-stack images. Representative images are included in the Supplemental Material [37]. In the second, we take advantage of the axisymmetric pore shape and use a quicker line scan across the diameter to obtain full knowledge of the location, curvature, and contact angle of the moving meniscus. This mode is applied to quantify the dynamic wetting process. The first scan at each liquid pressure started 5 min after the specimen was freshly immersed in water so that the system was allowed to settle. Subsequently, they are taken at regular intervals of 2–10 min depending on the applied liquid pressure (see Fig. 4 below). Each line scan beginning from below the bottom of the pore until reaching above the specimen surface consumes approximately 30 s. This time scale is much smaller than that of air diffusion, which we identify as the main mechanism driving meniscus progression (see below). Thus, the variation of the meniscus shape during each scan was negligible, and this mode allows us to acquire an optical image along the pore center plane.

The representative images with rhodamine-labeled water from the line-scanning mode are shown in Figs. 2(a)–2(d). Figures 2(a)–2(c) are first line scans taken 5 min after fresh immersion. The meniscus was almost planar in the absence of an applied pressure [$\Delta p = 0$ kPa, Fig. 2(a)]. As the liquid pressure increased to $\Delta p = 14$ kPa, the meniscus became concave but still pinned at the corner, i.e., in a CB state [Fig. 2(b)]. For this case, the bottom surface was hardly visible due to strong image distortion (discussed in the Supplemental Material [37]). At a much stronger liquid pressure of $\Delta p = 50$ kPa, the contact line depinned from the pore edges, which resulted in a metastable state [Fig. 2(c)]. When kept under 50 kPa for over 15 min, the air column gradually disappeared, leading to a W state [Fig. 2(d)]. Note that for this case, the pore was completely filled, although the fluorescence signal around the corners appeared to be weak, due to defocusing and optical reflection [37].

To avoid possible surfactant effects, we perform quantitative analysis of the metastable state and CB-W transition without adding the fluorescent dye. Figures 2(e)–2(h) show representative image detection which is solely due to reflection, and the resulted trends are comparable to those in Figs. 2(a)–2(d). Both the contact angle θ and the sagging depth h are measured from the 2D meniscus profiles [see Fig. 1(c)]. Note that in order to obtain true values for θ and h, the images in Figs. 2(a)–2(h) are corrected following a calibration method outlined in the Supplemental Material [37], which accounts for the effects of pressure-induced lens deflection.

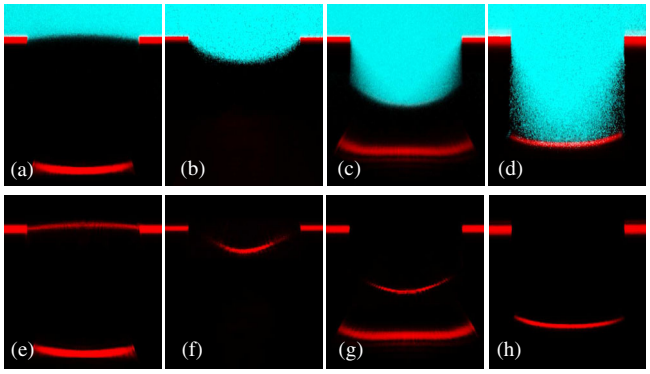

FIG. 2 (color online). Confocal microscopy images showing the meniscus 5 min after fresh immersion under 0 kPa (a),(e), 14 kPa (b),(f), 50 kPa (c),(g), and 15 min after immersion under 50 kPa (d),(h). Images in the first row were acquired with fluorescence-labeled water; the second row images were acquired without the dye. All images are corrected following a calibration method outlined in the Supplemental Material [37].

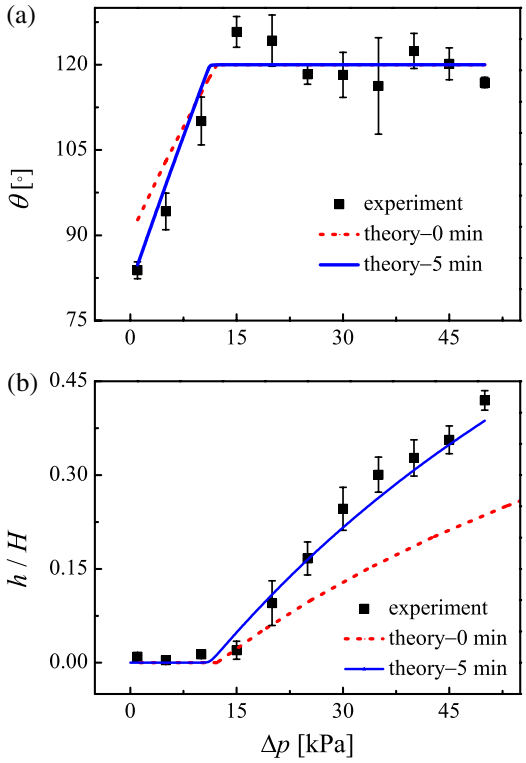

FIG. 3 (color online). Wetting transition induced by pressurization. Graphs show variations of (a) contact angle θ and (b) sagging depth h versus applied pressure Δp. Symbols: experimental data. Lines: theoretical predictions. The experimental measurements were performed 5 min after fresh immersion.

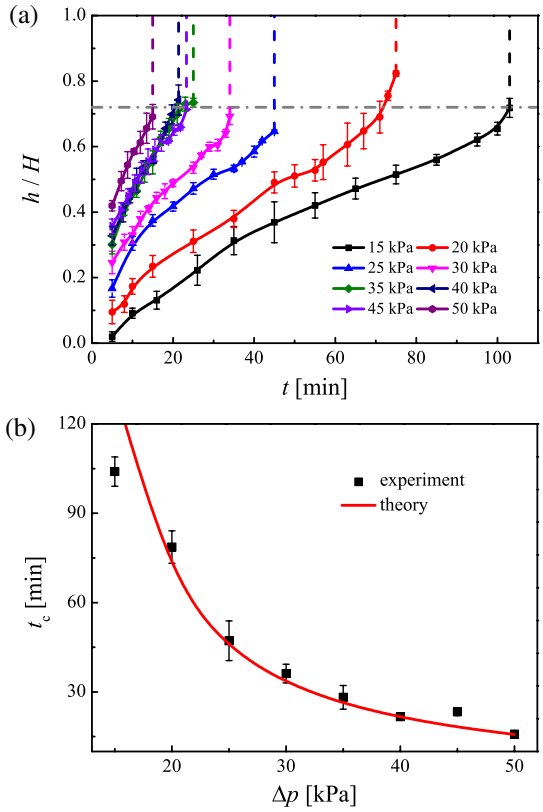

FIG. 4 (color online). (a) Experimental measurement of the dynamic evolution of the normalized sagging depth under different liquid pressures. The dot-dashed line shows the averaged collapse depth, $0.72H$. (b) The collapse time t_c, as a function of Δp. Symbols: experimental data. Solid: theoretical prediction.

Figure 3 shows the resulting values from the first line scan (5 min after fresh immersion) as a function of the applied pressure. All results below were obtained without fluorescence labeling. Both Figs. 3(a) and 3(b) exhibit a typical wetting transition character: at low Δp, θ increases monotonically and h remains unchanged, indicating pinning; at higher Δp, θ reaches a steady value, and the interface sags in deeper, as indicated by the increasing h. Figure 3 confirms the direct observation of the pinning CB and depinned metastable states as illustrated in Fig. 2. Figure 3(b) indicates that the depinning pressure is between $\Delta p = 12$ and 15 kPa. The average θ measured in the metastable states ($\Delta p > 15$ kPa) is approximately 120°, which is nothing but the advancing contact angle along the pore sidewall. In both figures, the lines are model predictions discussed in the sequel.

The dynamic advancing of the metastable state is examined in Fig. 4. In Fig. 4(a), we follow the sagging depth h, as a function of time for different applied pressures above $\Delta p = 15$ kPa. For all cases, $t = 0$ indicates fresh immersion, and the first point is available at $t = 5$ min. Clearly, h (normalized by the pore depth H) increases monotonically with time until the interface suddenly collapses. In the experiments, this collapse was characterized by a partial or complete merging of the interface with the bottom of the pore, at which moment the value h was no longer meaningful. This merging process, however, is not induced by a direct contact of the meniscus with the bottom due to its advancing. Indeed, the average sagging depth before collapsing is approximately $0.72H$ [see Fig. 4(a)] so that the distance between the center of the meniscus and the pore bottom is $0.17H$. Between the last measurement and the collapse, the meniscus was unlikely to traverse this distance at the (almost constant) projected rate of increase. We, therefore, speculate that the collapse is due to a loss of interfacial stability induced by surface energy minimization or triggered by local defects which are more prevalent close to the pore bottom.

The collapse time t_c as a function of the liquid pressure Δp is shown in Fig. 4(b). Here, t_c corresponds to the time for the last data point collected in Fig. 4(a). We can see that t_c decreases exponentially as the liquid pressure increases. This trend clearly indicates the limitation of structured superhydrophobic surfaces for submerged applications, especially under high liquid pressure. The disappearance of air inside cavities generally causes the failure of the surfaces in performing particular functions, e.g., drag reduction.

The above results elicit important observations that the metastable state possesses a finite life span, and the CB-W

transition is a gradual process depending on the system configuration. Below, we demonstrate that the dynamic transition is primarily mediated by the applied pressure along with gas diffusion. Detailed derivations follow our earlier work [22] and are presented in the Supplemental Material [37]. The key results are summarized here. In what follows, we assume a mechanical quasistatic equilibrium. First, the initial configuration of the meniscus is obtained by solving the Laplace equation and the equation of state for ideal gas:

$$p_L - p_V = \frac{p_{G,0}}{1 - h_0/H - (r/H)g(\theta_0)} - \frac{2\gamma\cos\theta_0}{r}. \quad (1)$$

Here, $g(\theta_0) = -[2 - 3\sin\theta_0 + \sin^3\theta_0]/3\cos^3\theta_0$, $p_{G,0}$ is the gas partial pressure at atmospheric pressure and is equal to $p_0 - p_V$, where p_V is the water vapor pressure. In Eq. (1), γ is the surface tension, and θ_0 and h_0 are the contact angle and sagging depth at fresh immersion, respectively. A critical pressure threshold for depinning is obtained by setting $h_0 = 0$ and $\theta_0 = \theta_a$, where θ_a is the constant advancing contact angle [Fig. 1(c); a measurement of θ_a on a flat surface hydrophobized with 1H,1H,2H,2H-Perfluorooctyltrichlorosilane is presented in the Supplemental Material [37]]. For the current study, this predicted threshold is $\Delta p = 12.5$ kPa, close to the measured value, 14 kPa (see Fig. 3). In a depinned state, θ_0 is set to be θ_a, and the initial sagging depth h_0 is determined from Eq. (1).

Once the initial configuration is obtained, the gas trapped in the pore exchanges with that dissolved in the bulk liquid via diffusion across a density-gradient-controlled boundary layer [33–36,38]. The evolution equation reads

$$\frac{d[p_G(t)V(t)]}{dt} = -\frac{A(t)D_G}{lK_G}[p_G(t) - sp_{G,0}], \quad (2)$$

where $p_G = p_L - p_V + 2\gamma\cos\theta/r$ is the gas partial pressure in the pore, A and V are the meniscus area and gas volume, and D_G and K_G are the diffusive coefficient and Henry's constant, respectively. Here, l is a characteristic diffusive length [38], and s represents the degree of gas saturation. For the pinned state, $h = 0$ in the calculation of A and V, and Eq. (2) governs the evolution of θ. In the depinned metastable state, $\theta = \theta_a$, and the rate of change for h becomes constant, as indicated by Eq. (2). A simple solution is obtained,

$$\frac{h(t)}{H} = \frac{h_0}{H} + \frac{A/\pi r^2}{K_G/RT}\left(\frac{t}{t_D}\right), \quad (3)$$

where a characteristic time scale emerges,

$$t_D = \frac{p_G}{(p_G - sp_{G,0})}\frac{Hl}{D_G}. \quad (4)$$

Here, Hl/D_G is a diffusive time scale, and the prefactor takes into account the pressure gradient in mediating gas exchange between the cavity and bulk water.

The saturation coefficient s of the bulk water in chamber 2 was measured to be 1.069 ± 0.017 [37], suggesting a slight oversaturation. The diffusion length l can be estimated using a classic formula, $l \sim \sqrt{D_G t}$, which reveals values in the mm range if we consider $t \sim 10^3$ s. The specific (phenomenological) value of l can be extracted from the experimental data. For the averaged collapsing depth of $h_c = 0.72H$, Eq. (3) gives a predicted average collapsing time, t_c. A least-squares fitting between the data and the prediction in Fig. 4(b) reveals $l = 0.45$ mm.

Theoretical predictions according to the above model are shown as lines in Fig. 3. The dashed lines are calculated using Eq. (1). The solid lines are calculated using Eq. (2), which takes into account gas diffusion in the 5-min interval between fresh immersion and the first line-scan measurement. Evidently, the solid lines present a good agreement between the data and the model prediction. Interestingly, in Fig. 3(a), the solid and dashed lines intersect. A physical interpretation is presented in the Supplemental Material [37].

The dimensionless solutions (3) and (4) provide a unified description of the progression of the metastable states under various pressure conditions. In Fig. 5, the data are rescaled with the characteristic time, t_D. The dimensionless sagging depth $(h - h_0)/H$ from all pressure conditions collapses well onto the single curve from the theoretical prediction (solid line). This agreement indicates that the simple model captures the main mechanism controlling the longevity of the air pockets, namely, gas diffusion under a pressure gradient across a thin boundary layer adjacent to the interface. Consequently, strategies such as decreasing p_G in the cavities following the Laplace equation or increasing the saturation degree s in the bulk water are expected to reduce the gas flux and enhance the lifetime of underwater superhydrophobic surfaces. The former can be achieved by using smaller structure sizes. For example, given a cylindrical pore size of $r = 2.5$ μm while keeping all other parameters the same as present, the collapse time can be increased from 15 to 60 min under a liquid pressure of 50 kPa. In addition, increasing the apparent contact angle of

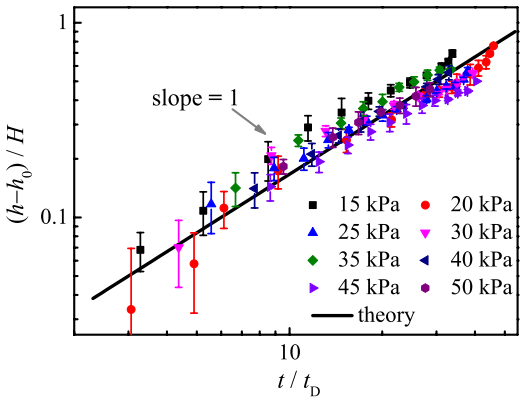

FIG. 5 (color online). Normalized sagging depth as a function of normalized time in the metastable states.

the meniscus with the sidewall also contributes to underwater longevity. This effect can be achieved by, e.g., surface treatment [39,40] and hierarchical structures [41,42]; the latter has been demonstrated to help sustain the metastable state [10]. Last but not least, although we used cylindrical-shaped pores as a model system, with an appropriate geometric equivalence method [22], the present theoretical framework can be generalized for analysis of more complicated surface structures (e.g., pillars). The current work, by combining quantitative measurements with theoretical analyses, provides a better prediction of the multiphase phenomenon pertinent to structure-enabled underwater superhydrophobicity.

The following agencies and programs are acknowledged: Major State Basic Research Development Program of China (Grant No. 2011CB013101), National Natural Science Foundation of China (NSFC) under Grants No. 11225208, No. 11172001, No. 10872003, and No. 11328201. H. L. acknowledges support from NSF Grant No. CBET-0747886. H. D. would like to acknowledge the Alexander von Humboldt (AvH) foundation in Germany for its support of this work through the project "Mechanics theory of materials with complex surfaces and its applications" in the frame of the AvH program for funding a research group linkage.

*Corresponding author.
hlin@jove.rutgers.edu
†Corresponding author.
hlduan@pku.edu.cn

[1] M. Nosonovsky and B. Bhushan, Curr. Opin. Colloid Interface Sci. **14**, 270 (2009).
[2] X. Zhang, F. Shi, J. Niu, Y. G. Jiang, and Z. Q. Wang, J. Mater. Chem. **18**, 621 (2008).
[3] N. Miljkovic and E. N. Wang, MRS Bull. **38**, 397 (2013).
[4] Y. H. Xue, H. J. Yuan, W. D. Su, Y. P. Shi, and H. L. Duan, Proc. R. Soc. A **470**, 20130832 (2014).
[5] A. B. D. Cassie and S. Baxter, Trans. Faraday Soc. **40**, 546 (1944).
[6] E. Bormashenko, R. Pogreb, G. Whyman, and M. Erlich, Langmuir **23**, 6501 (2007).
[7] M. Reyssat, J. M. Yeomans, and D. Quéré, Europhys. Lett. **81**, 26006 (2008).
[8] P. C. Tsai, R. G. H. Lammertink, M. Wessling, and D. Lohse, Phys. Rev. Lett. **104**, 116102 (2010).
[9] M. S. Bobji, S. V. Kumar, A. Asthana, and R. N. Govardhan, Langmuir **25**, 12120 (2009).
[10] R. Poetes, K. Holtzmann, K. Franze, and U. Steiner, Phys. Rev. Lett. **105**, 166104 (2010).
[11] M. A. Samaha, F. O. Ochanda, H. V. Tafreshi, G. C. Tepper, and M. Gad-el-Hak, Rev. Sci. Instrum. **82**, 045109 (2011).
[12] D. Bartolo, F. Bouamrirene, E. Verneuil, A. Buguin, P. Silberzan, and S. Moulinet, Europhys. Lett. **74**, 299 (2006).
[13] H. M. Kwon, A. T. Paxson, K. K. Varanasi, and N. A. Patankar, Phys. Rev. Lett. **106**, 036102 (2011).
[14] R. N. Wenzel, Ind. Eng. Chem. **28**, 988 (1936).
[15] S. Moulinet and D. Bartolo, Eur. Phys. J. E **24**, 251 (2007).
[16] M. Sbragaglia, A. M. Peters, C. Pirat, B. M. Borkent, R. G. H. Lammertink, M. Wessling, and D. Lohse, Phys. Rev. Lett. **99**, 156001 (2007).
[17] P. Papadopoulos, L. Mammen, X. Deng, D. Vollmer, and H. J. Butt, Proc. Natl. Acad. Sci. U.S.A. **110**, 3254 (2013).
[18] C. Luo, H. Zheng, L. Wang, H. P. Fang, J. Hu, C. H. Fan, Y. Cao, and J. A. Wang, Angew. Chem., Int. Ed. **49**, 9145 (2010).
[19] A. Marmur, Langmuir **20**, 3517 (2004).
[20] N. A. Patankar, Langmuir **20**, 7097 (2004).
[21] A. Dupuis and J. M. Yeomans, Langmuir **21**, 2624 (2005).
[22] Y. H. Xue, S. G. Chu, P. Y. Lv, and H. L. Duan, Langmuir **28**, 9440 (2012).
[23] A. Giacomello, M. Chinappi, S. Meloni, and C. M. Casciola, Phys. Rev. Lett. **109**, 226102 (2012).
[24] A. Tuteja, W. Choi, M. L. Ma, J. M. Mabry, S. A. Mazzella, G. C. Rutledge, G. H. McKinley, and R. E. Cohen, Science **318**, 1618 (2007).
[25] C. Lee and C. J. Kim, Phys. Rev. Lett. **106**, 014502 (2011).
[26] T. N. Krupenkin, J. A. Taylor, E. N. Wang, P. Kolodner, M. Hodes, and T. R. Salamon, Langmuir **23**, 9128 (2007).
[27] S. Adera, R. Raj, R. Enright, and E. N. Wang, Nat. Commun. **4**, 2518 (2013).
[28] P. Forsberg, F. Nikolajeff, and M. Karlsson, Soft Matter **7**, 104 (2011).
[29] T. Verho, J. T. Korhonen, L. Sainiemi, V. Jokinen, C. Bower, K. Franze, S. Franssila, P. Andrew, O. Ikkala, and R. H. A. Ras, Proc. Natl. Acad. Sci. U.S.A. **109**, 10210 (2012).
[30] L. Lei, H. Li, J. Shi, and Y. Chen, Langmuir **26**, 3666 (2010).
[31] J. B. Boreyko and C. H. Chen, Phys. Rev. Lett. **103**, 174502 (2009).
[32] P. C. Tsai, A. M. Peters, C. Pirat, M. Wessling, R. G. H. Lammertink, and D. Lohse, Phys. Fluids **21**, 112002 (2009).
[33] W. H. Thorpe, Biol. Rev. Camb. Philos. Soc. **25**, 344 (1950).
[34] H. Rahn and C. V. Charles, Respir. Physiol. **5**, 145 (1968).
[35] M. R. Flynn and J. W. M. Bush, J. Fluid Mech. **608**, 275 (2008).
[36] B. Emami, A. A. Hemeda, M. M. Amrei, A. Luzar, M. Gad-el-Hak, and H. V. Tafreshi, Phys. Fluids **25**, 062108 (2013).
[37] See Supplemental Material at http://link.aps.org/supplemental/10.1103/PhysRevLett.112.196101 for further details on 3D exemplary images, image-distortion correction, and theoretical derivations.
[38] J. H. Weijs and D. Lohse, Phys. Rev. Lett. **110**, 054501 (2013).
[39] L. C. Gao and T. J. McCarthy, J. Am. Chem. Soc. **128**, 9052 (2006).
[40] X. J. Liu, Y. M. Liang, F. Zhou, and W. M. Liu, Soft Matter **8**, 2070 (2012).
[41] L. Feng, S. H. Li, Y. S. Li, H. J. Li, L. J. Zhang, J. Zhai, Y. L. Song, B. Q. Liu, L. Jiang, and D. B. Zhu, Adv. Mater. **14**, 1857 (2002).
[42] N. J. Shirtcliffe, G. McHale, M. I. Newton, G. Chabrol, and C. C. Perry, Adv. Mater. **16**, 1929 (2004).